Current Biology 21, 1578–1583, September 27, 2011 ©2011 Elsevier Ltd All rights reserved DOI 10.1016/j.cub.2011.08.021

Report

Organization of the Smallest Eukaryotic Spindle

Lu Gan,[1] Mark S. Ladinsky,[1] and Grant J. Jensen[1,2,*]
[1]Division of Biology
[2]Howard Hughes Medical Institute
California Institute of Technology, Pasadena, CA 91125, USA

Summary

In metazoans, plants, and fungi, the spindle checkpoint delays mitosis until each chromosome is attached to one or more of its own kinetochore microtubules (kMTs). Some unicellular eukaryotes, however, have been reported to have fewer kMTs than chromosomes [1–5]. If this is the case, it is unclear how the spindle checkpoint could be satisfied. In the vast majority of the previous studies, mitotic cells were chemically fixed at room temperature, but this does not always preserve dynamic and/or small structures like spindle MTs and kinetochores [6]. Indeed, later higher-resolution studies have reversed some earlier claims [7–11]. Here we show that in *Ostreococcus tauri* (the smallest eukaryote known), mitosis does involve fewer spindle microtubules than chromosomes. *O. tauri* cultures were enriched for mitotic cells, high-pressure frozen, and then imaged in 3D both in plastic and in a near-native ("frozen-hydrated") state through electron tomography. Mitotic cells have a distinctive intranuclear heterochromatin-free "spindle tunnel" with approximately four short and occasionally one long, incomplete (unclosed) microtubule at each end of the spindle tunnel. Because other aspects of *O. tauri*'s spindle checkpoint seem typical, these data suggest that *O. tauri*'s 20 chromosomes are physically linked and segregated as just one or a small number of groups.

Results and Discussion

Detection and Enrichment of Mitotic Cells

The *Ostreococcus tauri* cell cycle can be loosely synchronized with light, resulting in early interphase cells at the dark-to-light transition (morning) and mitotic cells at the light-to-dark transition (evening) [12]. In our previous electron cryotomography study of evening cells, however, no spindles were detected [13]. At the time, we did not have a method to determine the percentage of mitotic cells, so we did not know whether mitotic cells were completely absent in those naturally synchronized samples or whether mitosis was simply so fast that none happened to be seen in our limited pool. We therefore developed an immunofluorescence assay to detect phosphohistone H3 [14], which is found in mitotic (H3P+) but not interphase (H3P−) cells (see Supplemental Results and Discussion and Figures S1A–S1C available online).

Using the H3P assay, we modified an artificial synchronization protocol that involved sequential drug treatments and washouts to arrest cells at successive stages of the cell cycle [15] (Table S1A; Supplemental Results and Discussion). Briefly, cells were first arrested at the G1/S transition with hydroxyurea, a DNA-synthesis inhibitor. Following a 9 hr incubation, the hydroxyurea was washed out and propyzamide, a tubulin polymerization inhibitor, was then added [16]. This allowed the cells to progress to prophase. Finally, following a 12 hr incubation, the propyzamide was washed out and replaced with the proteasome inhibitor MG132 [17]. This allowed the microtubules (MTs) to recover but arrested the cells in metaphase (39% mitotic cells; see Figure S1). Control experiments showed that the drug treatments were reversible and only slightly perturbed cell-culture viability (Figure S2). Together, these results indicate not only that *O. tauri* mitosis requires functional spindle MTs but also that the majority of propyzamide-arrested cells pass through mitosis within an hour after drug removal. Thus, the spindles in the "MG132-treated" cells imaged throughout the study must be functional.

Mitotic Nuclei Have Substantially Fewer than Forty Microtubules

MG132-treated cells were first imaged intact, plunge frozen (Figures S3A and S3B). Many of these cells were two or more times thicker than the mean free path of the electrons, however, reducing the quality of the tomographic reconstructions and restricting analysis to the smaller cells. None of these smaller cells exhibited a mitotic spindle.

To obtain images of the thicker, likely mitotic cells, cell pellets were high-pressure frozen, freeze substituted, plastic embedded, and sectioned. Tomograms of single plastic sections showed that MG132-treated cells were ovoid (1.5–2 μm long and ~1 μm wide), with the nucleus in the middle and chloroplasts at the cell poles (Figures S3C and S3D). Nuclei were ~0.7 μm wide. In the middle of mitotic nuclei, there was a heterochromatin-free zone that we refer to as the "spindle tunnel," which contained spindle MTs. The spindle tunnel flared out at its ends to 218 ± 16 nm (n = 16) and narrowed to only ~100 nm near its midpoint. Longitudinal sections (parallel to tunnel) showed that most spindle tunnels (7 of 10) contained one or two long, incomplete MTs (Figures S4A–S4C). Transverse sections (perpendicular to tunnel) through the ends of spindle tunnels consistently showed 4 ± 2 short MTs (n = 9), which often had C-shaped cross-sections (Figures S4D–S4F). No nuclear envelope was seen at the poles (the ends of the spindle tunnel where the spindle MTs terminated), suggesting that mitosis is semiopen. Centrosomes and spindle pole bodies were also not seen, and no astral MTs were detected in the cytoplasm outside the nucleus.

To obtain more complete views, we reconstructed the nuclei of four cells in their entirety by merging dual-axis tomograms from three or four serial 200 nm sections [18]. All four mitotic nuclei exhibited hourglass-shaped tunnels (Figure 1; Movie S1). Three of the four serially sectioned cells were sectioned nearly transverse to the tunnel (Figures 1A–1C) and contained several short spindle MTs at the poles. These short MTs (<100 nm) were roughly parallel and clustered together, with nearest-neighbor distances of 40–50 nm. Additionally, incomplete long MTs penetrated into the middle of three of the tunnels (Figure 1A, row 1), in some cases almost reaching the opposite pole (Figure 1D), likely serving as polar MTs analogous to the long MTs in other eukaryotes. Negative-control

*Correspondence: jensen@caltech.edu

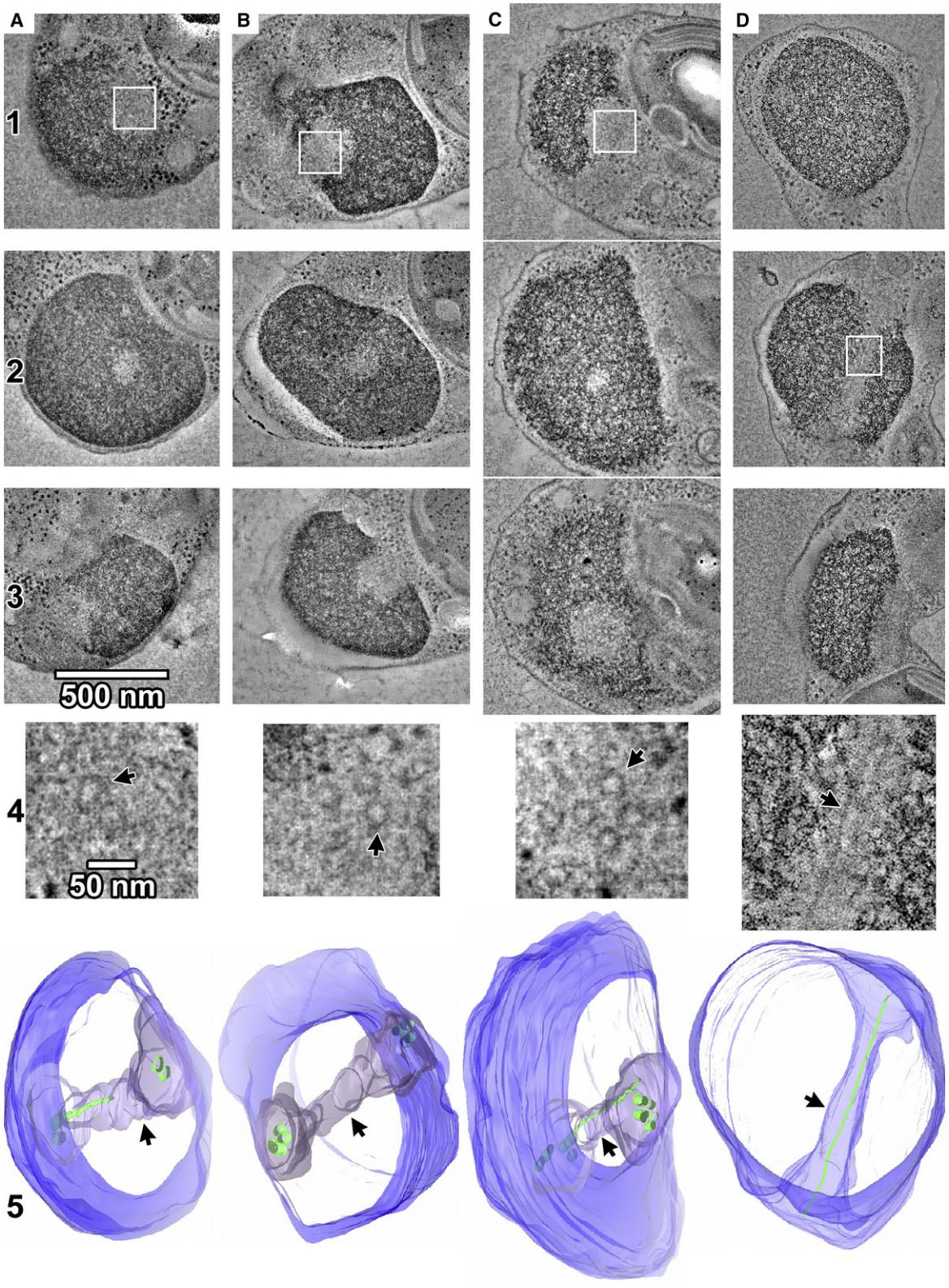

Figure 1. *O. tauri* Has Only a Few Spindle Microtubules

Tomographic slices (19 nm thick) through merged serial-section tomograms of MG132-treated, high-pressure-frozen, freeze-substituted *O. tauri* cells. The entire nuclei and spindles are reconstructed in the merged tomogram. The cells in (A)–(C) were sectioned nearly transverse to the spindle tunnel and the cell in (D) nearly longitudinal. Rows 1–3 show tomographic slices through upper, middle, and lower plastic sections of the nucleus. Row 4 shows enlargements of the areas boxed in white in rows 1 or 2, with small rotations out of plane to enhance the visibility of the spindle microtubules (MTs). Arrows in row 4 indicate example MTs. Row 5 shows 3D segmentations of the chromatin boundary (blue), spindle tunnel (arrowheads), and MTs (green). Note that the tunnel-spanning portions of long MTs have incomplete walls and are modeled as thin rods instead of tubes. The cell in (B) is shown in greater detail in Movie S1.

tomograms of interphase cells confirmed that spindle tunnels were only found in mitotic cells (Figures S4G and S4H; Supplemental Results and Discussion).

O. tauri Spindle Microtubules Are Rarely Complete Tubes

To obtain higher-resolution images of the spindles in a closer-to-native state, we cryosectioned high-pressure-frozen MG132-treated cells and imaged them in a near-native, "frozen-hydrated" state. Cells were selected at random because neither the spindle tunnel nor spindle MTs could be seen in the low-dose low-magnification images used to locate cells for cryotomography. Each cryosection (nominally ~150 nm thick) contained only ~1/4th to 1/5th of the typically ~700 nm-wide nucleus, meaning that only a random portion of a spindle could be imaged in each tomogram. Cryosections taken transverse to the spindle axis and near the pole were the most informative because they provide the most accurate estimate of MTs in a half spindle. Several hundred (356) cryosections were imaged and analyzed to ensure that no structures were missed (Table S1). Portions of spindles were found in 44 cryosections, organized into small clusters of parallel MTs (Figure 2). None of the clusters had more than five MTs, confirming the low numbers seen in the plastic sections.

The resolution of the cryosection tomograms was sufficient to discern individual protofilaments (Figure 2; Figure 3; Table S2). Although occasionally one or two long (>200 nm) MTs were seen, the majority of the spindle MTs were shorter than 100 nm (15 of 24 not truncated by the cryosectioning), corresponding to less than 12 (8 nm long) α-β tubulin dimers. Some MTs were only ~50 nm long (Figure 3, MTs 10, 19, and 20), corresponding to just a few α-β tubulin dimers. When the end structures were clear, MTs were seen to have one conical and one open end (Figure 3, MTs 10, 19, and 26) or two open ends (MTs 14 and 20). Whereas the conical caps were likely the cone-shaped γ-tubulin complex [19], the MTs with two open ends may have been nucleated by some γ-tubulin-independent mechanism as has been observed in other organisms [20, 21]. Because neither spindle pole bodies nor centrosomes were seen, as has been the case in various plant cells [22], it remains to be determined how *O. tauri* spindle MTs organize at the poles.

Most of the MTs had fewer than 13 protofilaments (4 to 12) and had C-shaped cross-sections. MTs with C-shaped cross-sections have been found in the spindles of other organisms [23–25], but the short C-shaped region (0.1–0.5 μm long) was located at the plus ends of MTs, often near the middle of the spindles. MTs with the fewest protofilaments—as few as four (Figure 3, MT 8)—had flatter cross-sections. Side views of these MTs often showed a slight curve along the protofilament axis. We did not observe MT protofilaments in the highly curved "ram's horn" motif that has been reported for MTs shrinking in vitro [26, 27]. While the structure of *O. tauri* MTs was reminiscent of the nearly flat sheets seen at the plus ends of MTs growing in vitro [26, 27], recent electron tomography studies have shown that MTs growing in vivo have flared plus-end morphologies instead [28, 29]. Therefore, although the MTs were likely undergoing rapid dynamics, we cannot conclude whether the *O. tauri* spindle MTs were growing or shrinking based on their morphology.

The Spindle Microtubules Seen Were Likely Functional Mitotic Structures

Control experiments confirmed that spindle MTs were exclusive to mitotic (H3P+) cells (Supplemental Results and Discussion). To check whether the MG132 treatment was influencing the appearance of the spindle MTs, causing them to appear incomplete, we analyzed the structures of cytoplasmic MTs in the same cells. Cytoplasmic MTs in the MG132-treated cells appeared complete in tomographic slices perpendicular to the MT axis and had the 25 nm-wide double-line motif in tomographic slices parallel to the MT axis (Figure 3), just like the cytoplasmic MTs seen in plunge-frozen interphase *O. tauri* cells [13] and cells long after the propyzamide was washed out. This proves that the tubulin in these cells was able to form complete MTs. Cryotomograms of cells that were high-pressure frozen between 10 and 20 min after propyzamide washout and without MG132 treatment also showed the same characteristics of low number (~4), short length (<100 nm), and frequent lack of complete walls. Many of these were in the midst of mitosis, because immunofluorescence images showed that 50% (n = 252) of the cells were H3P+ before the high-pressure-freezing step and only 26% (n = 261) of the cells were H3P+ afterward. MG132 therefore does not appear to influence the structure of spindle MTs.

O. tauri Has Less Than One Microtubule per Chromosome

Although it has been claimed in the past that certain unicellular eukaryotes undergo mitosis with fewer MTs than chromosomes, uncertainties in the number of chromosomes and limitations of traditional electron microscopy techniques to preserve short MTs and small kinetochores has left considerable room for doubt (Supplemental Results and Discussion). Using tomography of rapidly frozen cells, including cryosectioned cells preserved in the frozen-hydrated state, we here observed that mitotic *O. tauri* cells exhibited far fewer spindle MTs (~10) than chromosomes [30]. The spindle MTs were arranged as a small cluster of approximately four short, incomplete MTs at each spindle pole and one or two long MTs extending into a spindle tunnel (Figure 4). Furthermore, because (1) the spindle poles were so small (~200 nm diameter), (2) the center-to-center MT spacing varied between 40 and 50 nm, and (3) there was no apparent ordered packing, there simply was not enough room for many more MTs. Because the difference between the number of chromosomes and spindle MTs counted was so great and the total number of partial and full spindles imaged was so large (13 partial and 4 full spindles in plastic sections; 64 partial spindles in cryosections), it is very unlikely that our survey would have missed a full (21-MT) half-spindle, had it existed. We conclude that *O. tauri* segregates its chromosomes with less than one MT per chromosome.

Possible Mechanisms for *O. tauri* Chromosome Segregation

Another class of photosynthetic plankton, the diatoms, reportedly uses an actin/myosin-based spindle "matrix" to move its chromosomes to the spindle poles and keep them there until the end of mitosis [31] (Supplemental Results and Discussion). Although actin-like filaments are routinely visible in cryotomograms of small cells [32, 33], no such matrix was seen here in *O. tauri*. *O. tauri* mitosis was also clearly MT dependent, because it was arrested by propyzamide, an inhibitor of tubulin polymerization.

Kinetochores were also not identified in the tomograms, but two lines of evidence suggest that *O. tauri* chromosomes possess them. First, all known MT-related mitotic arrests are caused by the spindle checkpoint, which is generated by kinetochores [34]. Because *O. tauri* mitosis was arrested by

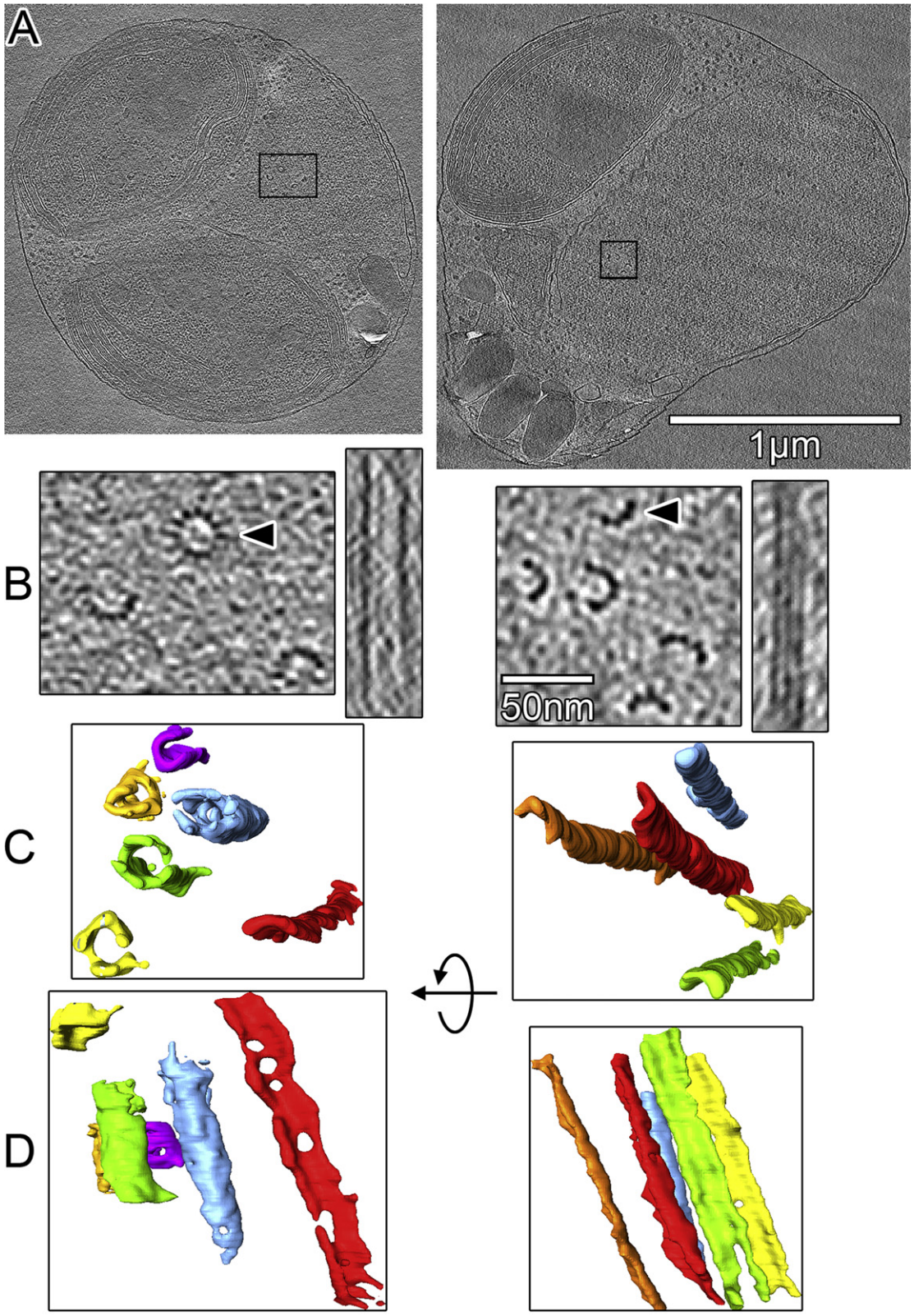

Figure 2. *O. tauri* Spindle Microtubules Are Short and Mostly Incomplete

(A) Tomographic slices (20 nm thick) through cryotomograms of vitreously sectioned MG132-treated cells.

(B) Enlarged view of the spindle MT clusters boxed in (A). The right subpanels show longitudinal slices of the MTs indicated by the arrowheads, taken through the center of the MT barrel (left cell) or along three protofilaments (right cell).

(C and D) Segmentations of the spindle MTs in (B), colored randomly for clarity. The apparent "holes" in the MT walls are likely artifacts of the low signal-to-noise ratio.

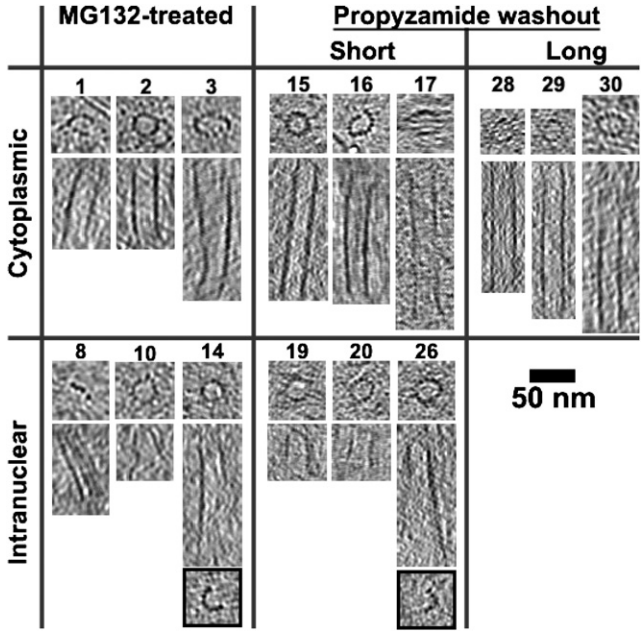

Figure 3. Example Microtubules from Cryosectioned Cells

Tomographic slices (10 or 20 nm thick) through many MTs taken perpendicular (upper subpanels) and parallel (lower subpanels) to the MT axis. MTs 14 and 26 are complete, with 13 protofilaments at one end (top subpanel) but not the other (lower subpanels with black border). In contrast to cytoplasmic MTs, which have long, complete walls, most of the intranuclear (spindle) MTs are short and C-shaped along most of their length. MTs 10, 19, and 26 have one conical and one open end; MTs 14 and 20 have two open ends. Some MTs are only ~50 nm long (MTs 10, 19, and 20), which would consist of just a few α-β tubulin dimers (8 nm long). *O. tauri* spindle MTs are in general short with C-shaped profiles along most of their length, which is in agreement with the short MTs observed in the plastic-sectioned cells. See Table S2 for additional example MTs.

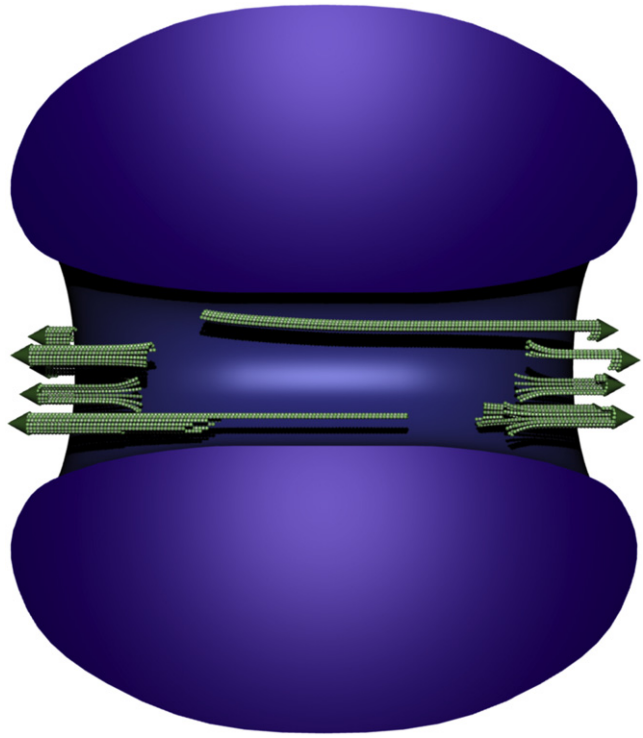

Figure 4. Organization of the *O. tauri* Spindle

Scale model of the *O. tauri* spindle in the context of the chromatin, shown in longitudinal cross-section. A small bundle of incomplete MTs (green) reside at each pole, and up to one long, incomplete MT extends deep into the nucleus from each pole. Heterochromatin (blue) forms a torus-like structure with a central channel that we call the spindle tunnel. Individual chromosomes could not be resolved. The nuclear envelope (not shown) has openings at both spindle poles.

propyzamide, it likely has a spindle checkpoint. Second, homologs of many kinetochore genes are present in the *O. tauri* genome, including *Nuf2*, *Ndc80*, *CENP-C*, *Bub3*, *Mad2*, *Mad3*, *Cdc20*, Aurora B, *Bub1*, *Mad1*, Polo kinases, and a *CenH3* candidate [30]. We have now shown that *O. tauri* at least has a functional Aurora B kinase, because the mitotic cells have the H3P epitope, which is generated by Aurora B in other eukaryotes [35]. *O. tauri*'s kinetochores were probably too small to be recognized, perhaps like the tiny *Saccharomyces cerevisiae* "point" kinetochores [36], which have also not yet been observed by electron microscopy [37].

How then does *O. tauri* segregate its 20 chromosome pairs with so few kinetochore microtubules (kMTs)? At least two possibilities should be considered. First, individual kMTs or the entire kMT bundle might attach to a single chromosome and move chromosomes one or a few at a time. Such a mechanism would require major adaptations, however, like tethering segregated chromosomes to the spindle pole and then resetting the spindle checkpoint. We are not aware of any precedent for this and judge the required complexities unlikely. In the second model, if the twenty nonhomologous chromosomes were physically linked at metaphase, they could be segregated together by a smaller number of kMTs. The spindle checkpoint could be satisfied if each chromosome (with its own checkpoint-signaling complex) attached to a common kinetochore, possibly akin to kinetochore clustering in *Schizosaccharomyces pombe* and maize [38, 39] (Supplemental Results and Discussion). This model might also explain chromosome segregation in *Trypanosoma brucei* (~27 larger chromosomes and ~8 kinetochores; see Supplemental Results and Discussion) and other picoplankton [40, 41].

Supplemental Information

Supplemental Information includes Supplemental Results and Discussion, four figures, three tables, Supplemental Experimental Procedures, and one movie and can be found with this article online at doi:10.1016/j.cub.2011.08.021.

Acknowledgments

We thank G. Henderson, P. Dias, A. McDowall, F.-Y. Bouget, H. Moreau, W. Marshall, J. Azimzadeh, and G. Ou for discussions and the anonymous reviewers for helpful comments. This work was supported in part by National Institutes of Health (NIH) grant P50 GM082545 to G.J.J. and a gift to the California Institute of Technology from the Gordon and Betty Moore Foundation. L.G. is a Damon Runyon Fellow supported by a fellowship from the Damon Runyon Cancer Research Foundation (DRG-1940-07). M.S.L. was supported by NIH grant 2 R37 AI041239-06A1 to P. Björkman.

Received: November 4, 2010
Revised: June 17, 2011
Accepted: August 9, 2011
Published online: September 8, 2011

References

1. Grell, K. (1973). Protozoology: With 15 Tab (Berlin: Springer).
2. Kubai, D.F. (1975). The evolution of the mitotic spindle. Int. Rev. Cytol. *43*, 167–227.
3. Heath, I.B. (1980). Variant mitoses in lower eukaryotes: Indicators of the evolution of mitosis. Int. Rev. Cytol. *64*, 1–80.
4. Raikov, I.B. (1982). The Protozoan Nucleus: Morphology and Evolution (Vienna: Springer-Verlag).
5. Daniels, J.P., Gull, K., and Wickstead, B. (2010). Cell biology of the trypanosome genome. Microbiol. Mol. Biol. Rev. *74*, 552–569.
6. McDonald, K.L., and Auer, M. (2006). High-pressure freezing, cellular tomography, and structural cell biology. Biotechniques *41*, 137–143.
7. Franke, W.W., and Reau, P. (1973). The mitotic apparatus of a zygomycete, Phycomyces blakesleeanus. Arch. Mikrobiol. *90*, 121–129.
8. McCully, E.K., and Robinow, C.F. (1973). Mitosis in Mucor hiemalis. A comparative light and electron microscopical study. Arch. Mikrobiol. *94*, 133–148.
9. Heath, I.B., and Rethoret, K. (1982). Mitosis in the fungus Zygorhynchus moelleri: Evidence for stage specific enhancement of microtubule preservation by freeze substitution. Eur. J. Cell Biol. *28*, 180–189.
10. McCully, E.K., and Robinow, C.F. (1971). Mitosis in the fission yeast Schizosaccharomyces pombe: a comparative study with light and electron microscopy. J. Cell Sci. *9*, 475–507.
11. Ding, R., McDonald, K.L., and McIntosh, J.R. (1993). Three-dimensional reconstruction and analysis of mitotic spindles from the yeast, Schizosaccharomyces pombe. J. Cell Biol. *120*, 141–151.
12. Farinas, B., Mary, C., de O Manes, C.L., Bhaud, Y., Peaucellier, G., and Moreau, H. (2006). Natural synchronisation for the study of cell division in the green unicellular alga Ostreococcus tauri. Plant Mol. Biol. *60*, 277–292.
13. Henderson, G.P., Gan, L., and Jensen, G.J. (2007). 3-D ultrastructure of O. tauri: Electron cryotomography of an entire eukaryotic cell. PLoS ONE *2*, e749.
14. Hendzel, M.J., Wei, Y., Mancini, M.A., Van Hooser, A., Ranalli, T., Brinkley, B.R., Bazett-Jones, D.P., and Allis, C.D. (1997). Mitosis-specific phosphorylation of histone H3 initiates primarily within pericentromeric heterochromatin during G2 and spreads in an ordered fashion coincident with mitotic chromosome condensation. Chromosoma *106*, 348–360.
15. Corellou, F., Camasses, A., Ligat, L., Peaucellier, G., and Bouget, F.Y. (2005). Atypical regulation of a green lineage-specific B-type cyclin-dependent kinase. Plant Physiol. *138*, 1627–1636.
16. Akashi, T., Izumi, K., Nagano, E., Enomoto, M., Mizuno, K., and Shibaoka, H. (1988). Effects of propyzamide on tobacco cell microtubules in vivo and in vitro. Plant Cell Physiol. *29*, 1053–1062.
17. Genschik, P., Criqui, M.C., Parmentier, Y., Derevier, A., and Fleck, J. (1998). Cell cycle-dependent proteolysis in plants. Identification of the destruction box pathway and metaphase arrest produced by the proteasome inhibitor mg132. Plant Cell *10*, 2063–2076.
18. Ladinsky, M.S., Mastronarde, D.N., McIntosh, J.R., Howell, K.E., and Staehelin, L.A. (1999). Golgi structure in three dimensions: Functional insights from the normal rat kidney cell. J. Cell Biol. *144*, 1135–1149.
19. Moritz, M., Braunfeld, M.B., Guénebaut, V., Heuser, J., and Agard, D.A. (2000). Structure of the gamma-tubulin ring complex: A template for microtubule nucleation. Nat. Cell Biol. *2*, 365–370.
20. Mahoney, N.M., Goshima, G., Douglass, A.D., and Vale, R.D. (2006). Making microtubules and mitotic spindles in cells without functional centrosomes. Curr. Biol. *16*, 564–569.
21. Kitamura, E., Tanaka, K., Komoto, S., Kitamura, Y., Antony, C., and Tanaka, T.U. (2010). Kinetochores generate microtubules with distal plus ends: Their roles and limited lifetime in mitosis. Dev. Cell *18*, 248–259.
22. Wasteneys, G.O. (2002). Microtubule organization in the green kingdom: Chaos or self-order? J. Cell Sci. *115*, 1345–1354.
23. Cohen, W.D., and Gottlieb, T. (1971). C-microtubules in isolated mitotic spindles. J. Cell Sci. *9*, 603–619.
24. Jensen, C., and Bajer, A. (1973). Spindle dynamics and arrangement of microtubules. Chromosoma *44*, 73–89.
25. McIntosh, J.R., Roos, U.P., Neighbors, B., and McDonald, K.L. (1985). Architecture of the microtubule component of mitotic spindles from Dictyostelium discoideum. J. Cell Sci. *75*, 93–129.
26. Mandelkow, E.M., Mandelkow, E., and Milligan, R.A. (1991). Microtubule dynamics and microtubule caps: A time-resolved cryo-electron microscopy study. J. Cell Biol. *114*, 977–991.
27. Chrétien, D., Fuller, S.D., and Karsenti, E. (1995). Structure of growing microtubule ends: Two-dimensional sheets close into tubes at variable rates. J. Cell Biol. *129*, 1311–1328.
28. Höög, J.L., Huisman, S.M., Sebö-Lemke, Z., Sandblad, L., McIntosh, J.R., Antony, C., and Brunner, D. (2011). Electron tomography reveals a flared morphology on growing microtubule ends. J. Cell Sci. *124*, 693–698.
29. Kukulski, W., Schorb, M., Welsch, S., Picco, A., Kaksonen, M., and Briggs, J.A. (2011). Correlated fluorescence and 3D electron microscopy with high sensitivity and spatial precision. J. Cell Biol. *192*, 111–119.
30. Derelle, E., Ferraz, C., Rombauts, S., Rouzé, P., Worden, A.Z., Robbens, S., Partensky, F., Degroeve, S., Echeynié, S., Cooke, R., et al. (2006). Genome analysis of the smallest free-living eukaryote Ostreococcus tauri unveils many unique features. Proc. Natl. Acad. Sci. USA *103*, 11647–11652.
31. Falciatore, A., and Bowler, C. (2002). Revealing the molecular secrets of marine diatoms. Annu. Rev. Plant Biol. *53*, 109–130.
32. Komeili, A., Li, Z., Newman, D.K., and Jensen, G.J. (2006). Magnetosomes are cell membrane invaginations organized by the actin-like protein MamK. Science *311*, 242–245.
33. Swulius, M.T., Chen, S., Jane Ding, H., Li, Z., Briegel, A., Pilhofer, M., Tocheva, E.I., Lybarger, S.R., Johnson, T.L., Sandkvist, M., and Jensen, G.J. (2011). Long helical filaments are not seen encircling cells in electron cryotomograms of rod-shaped bacteria. Biochem. Biophys. Res. Commun. *407*, 650–655.
34. Rieder, C.L., and Maiato, H. (2004). Stuck in division or passing through: What happens when cells cannot satisfy the spindle assembly checkpoint. Dev. Cell *7*, 637–651.
35. Prigent, C., and Dimitrov, S. (2003). Phosphorylation of serine 10 in histone H3, what for? J. Cell Sci. *116*, 3677–3685.
36. Joglekar, A.P., Bouck, D.C., Molk, J.N., Bloom, K.S., and Salmon, E.D. (2006). Molecular architecture of a kinetochore-microtubule attachment site. Nat. Cell Biol. *8*, 581–585.
37. Winey, M., Mamay, C.L., O'Toole, E.T., Mastronarde, D.N., Giddings, T.H., Jr., McDonald, K.L., and McIntosh, J.R. (1995). Three-dimensional ultrastructural analysis of the Saccharomyces cerevisiae mitotic spindle. J. Cell Biol. *129*, 1601–1615.
38. Appelgren, H., Kniola, B., and Ekwall, K. (2003). Distinct centromere domain structures with separate functions demonstrated in live fission yeast cells. J. Cell Sci. *116*, 4035–4042.
39. Li, X., and Dawe, R.K. (2009). Fused sister kinetochores initiate the reductional division in meiosis I. Nat. Cell Biol. *11*, 1103–1108.
40. Matsuzaki, M., Misumi, O., Shin-I, T., Maruyama, S., Takahara, M., Miyagishima, S.Y., Mori, T., Nishida, K., Yagisawa, F., Nishida, K., et al. (2004). Genome sequence of the ultrasmall unicellular red alga Cyanidioschyzon merolae 10D. Nature *428*, 653–657.
41. Worden, A.Z., Lee, J.H., Mock, T., Rouzé, P., Simmons, M.P., Aerts, A.L., Allen, A.E., Cuvelier, M.L., Derelle, E., Everett, M.V., et al. (2009). Green evolution and dynamic adaptations revealed by genomes of the marine picoeukaryotes Micromonas. Science *324*, 268–272.